RESEARCH ARTICLE

Early Changes in Striatal Activity and Motor Kinematics in a Huntington's Disease Mouse Model

Ellen T. Koch, BSc,[1,2] Marja D. Sepers, PhD,[1] Judy Cheng, BSc,[1,2] and Lynn A. Raymond, MD, PhD[1*]

[1]*Department of Psychiatry, Djavad Mowafaghian Centre for Brain Health, University of British Columbia, Vancouver, BC, Canada*
[2]*Graduate Program in Neuroscience, University of British Columbia, Vancouver, BC, Canada*

ABSTRACT: Background: Huntington's disease is a progressive neurodegenerative disorder with no disease-modifying treatments. Patients experience motor, cognitive, and psychiatric disturbances, and the dorsal striatum is the main target of neurodegeneration. Mouse models of Huntington's disease show altered striatal synaptic signaling in vitro, but how these changes relate to behavioral deficits in vivo is unclear.

Objectives: We aimed to investigate how striatal activity correlates with behavior in vivo during motor learning and spontaneous behavior in a Huntington's disease mouse model at two disease stages.

Methods: We used fiber photometry to record jGCaMP7f fluorescence, a read-out of neuronal activity, in the dorsal striatum of YAC128 (yeast artificial chromosome-128CAG) mice during accelerating rotarod and open-field behavior.

Results: Mice showed increased striatal activity on the rotarod, which diminished by late stages of learning, leading to an inverse correlation between latency to fall and striatal activity. The 2- to 3-month-old YAC128 mice did not show a deficit in latency to fall, but displayed significant differences in paw kinematics, including increased paw slip frequency and variability in paw height. These mice exhibited a weaker correlation between latency to fall and striatal activity and aberrant striatal activity during paw slips. At 6 to 7 months, the YAC128 mice showed significantly reduced latency to fall, impaired paw kinematics, and increased striatal activity while on the rotarod. In the open field, the YAC128 mice showed elevated neuronal activity at rest.

Conclusions: We uncovered impaired motor coordination at a stage thought to be premotor manifest in YAC128 mice and aberrant striatal activity during the accelerating rotarod and open-field exploration. © 2022 The Authors. *Movement Disorders* published by Wiley Periodicals LLC on behalf of International Parkinson and Movement Disorder Society

Key Words: huntington; striatum; basal ganglia; motor learning; rotarod

The striatum is the input hub of the basal ganglia, receiving glutamatergic projections from the cortex and thalamus and dopaminergic projections from the substantia nigra. Studies conducted in humans and animals highlight the importance of corticostriatal signaling, and especially the dorsal striatum, in action selection and motor learning.[1–4] The dorsal striatum is the primary site of neurodegeneration in the heritable movement disorder Huntington's disease (HD) along with cortical degeneration.[5,6] Patients with HD suffer from loss of motor control, including impaired fine motor coordination, chorea, and motor-learning deficits.[5,6]

The YAC128 (Yeast artificial chromosome-128CAG) transgenic mouse model expresses a full-length human mutant huntingtin gene and develops a progressive behavioral phenotype, corticostriatal synaptic dysfunction, and reduced cortical and striatal volume.[7–9] Notably, YAC128 mice display plasticity deficits at corticostriatal synapses

*__Correspondence to:__ Dr. Lynn A. Raymond, Djavad Mowafaghian Centre for Brain Health, Room 3408C 2215 Wesbrook Mall, Vancouver, BC V6T 1Z3, Canada; E-mail: lynn.raymond@ubc.ca

Relevant conflicts of interest/financial disclosures: No conflicts of interest to report.

Funding agencies: Funding was provided by the Canadian Institutes of Health Research (FDN-143210) to L.A.R. E.T.K. was supported by the University of British Columbia Four Year Fellowship and Canadian Open Neuroscience Platform.

Received: 31 March 2022; **Revised:** 26 May 2022; **Accepted:** 30 June 2022

Published online 26 July 2022 in Wiley Online Library (wileyonlinelibrary.com). DOI: 10.1002/mds.29168

starting at 6 weeks, including impaired activity-dependent endocannabinoid (eCB)-mediated long-term depression (eCB-LTD) in an acute brain slice.[10] Synaptic plasticity and eCB signaling in the striatum have been implicated in various forms of learning.[11] YAC128 mice also show changes in corticostriatal glutamate and nigrostriatal dopamine transmission.[9,12,13]

YAC128 mice exhibit progressive impairments on the rotarod, an assay of motor learning and coordination.[7,8] In normal animals, studies have reported plastic changes in the motor cortex and dorsal striatum associated with rotarod learning.[2,14–17] Aberrant corticostriatal signaling and plasticity could contribute to rotarod deficits and other behavioral changes in YAC128, but few studies have assessed neural activity in vivo during behavior in HD mice. Elevated low-frequency gamma power measured by local field potentials has been reported in the striatum of R6/2 and zQ175 mouse models of HD at rest.[18–20] The synchrony of high-frequency activity between the motor cortex and dorsal striatum during natural behaviors is impaired in R6/2 mice,[18] and elevated striatal spiny projection neuron (SPN) firing has been observed along with disrupted correlated firing between SPNs.[21] A recent study found striosomal circuit decline in the striatum of HD mice, accompanied by impaired valence-based learning.[22] To date, no study has investigated how striatal activity is affected in vivo during motor learning in HD mice.

Here, we used fiber photometry to measure jGCaMP7f activity in the dorsal striatum of YAC128 mice and their wild-type (WT) littermates during rotarod learning and open-field exploration. This work provides insights into striatal encoding of motor learning and spontaneous behavior, reveals impaired paw kinematics in YAC128 mice, and uncovers aberrant striatal signaling at different disease stages.

Materials and Methods

Experimental Animals

Animals were group housed on a 12:12 hour light–dark cycle with access to food and water ad libitum and provided with nesting material, a plastic tube, and cardboard hut. The 2- to 3-month-old and 6- to 7-month-old male heterozygous YAC128 animals were compared with male Friend Virus B/NIH (FVB/N strain) littermates. Procedures were performed in accordance with the Canadian Council on Animal Care and approved by the University of British Columbia Animal Care Committee (Protocol A19-0076).

Surgeries and Histology

Stereotaxic viral injections were performed as described previously.[23] Mice were injected with AAV9.syn.jGCaMP7f.WPRE (titer ≥1 $\times 10^{13}$ vg/mL, 1 μL, AddGene, provided by Douglas Kim, Janelia Farm Research Campus, Ashburn, VA) or AAV5.hSyn.EGFP (titer ≥7 $\times 10^{12}$ vg/mL, 1 μL, AddGene, provided by Bryan Roth) into the dorsal striatum (Anterior/posterior + 0.7, medial/lateral + 2.25, dorsal/ventral −3.0). A 400-μm core 0.57 NA optical fiber (Doric) was implanted in the same location and secured with dental cement. Mice were returned to group housing, and experiments were performed after 2 weeks. For histological assessment, the brain was sliced using a vibratome (VT1000 Leica, Wetzlar, Germany). Slices were then either preserved in 4% paraformaldehyde and mounted for imaging with an epifluorescence microscope (Zeiss, Oberkochen, Germany) or placed in room-temperature artificial cerebrospinal fluid immediately following slicing and imaged using a charge-coupled device camera (Dalsa, Waterloo, Canada).

Fiber Photometry Apparatus

The fiber photometry setup consisted of a RZ5P processor (TDT, Alachua, FL), two Light-Emitting Diodes (465 nm and 405 nm; Doric, 357 rue Franquet, Quebec, Canada), four-port fluorescence minicube (Doric), photoreceiver (Newport, Irvine, CA), and several mono-fiber-optic patch cords and Bayonet Neil-Concelman (BNC) cables (Doric). The 405 nm LED excites jGCaMP7f near its isosbestic point, used to control for bleaching and motion artifacts in the calcium-dependent jGCaMP7f signal (465 nm excitation). Emission wavelengths were sent back to the photoreceiver, which connected to the RZ5P where the two emissions were separated by lock-in modulation. Synapse software (TDT) was used to control experimental parameters and collect data.

Accelerating Rotarod

Mice were habituated to handling and being attached to the fiber-optic patch cord ahead of experiments. Mice learned to run when placed on a rotating rod (Ugo Basile, Lombardy, Italy) that accelerated from 5 to 40 rpm for 300 seconds. When they fell, the rotarod was stopped by a sensor or manually by the experimenter. For some trials, the mice rotated around the rotarod instead of falling, considered equivalent to a fall. Mice performed three trials/day for 4 days with a 1.5- to 2-hour intertrial interval. The rotarod was connected to the RZ5P through a parallel port that aligned the start and end of the trial with jGCaMP7f signals. Before and after each trial, we recorded 5 minutes of jGCaMP7f activity while mice freely explored an empty cage (17 × 28 cm). Webcams (Logitech, Newark, CA) were used to video the mouse's paws on the rotarod and behavior in the empty cage.

Open Field

Mice explored a 12 × 15" empty cage for 10 minutes per session over 3 or 4 days. A webcam was placed above to video the animal's behavior, and the fiber-optic patch cord was suspended above the empty cage.

jGCaMP7f Analysis

jGCaMP7f data were analyzed with several MATLAB (Natick, MA) scripts and functions (TDT and in house; https://github.com/orgs/ubcbraincircuits/repositories). To calculate the percentage change in fluorescence (%Δ*F*/*F*0), the isosbestic signal was first linearly fitted to the calcium-dependent signal. Then, %Δ*F*/*F*0 was calculated using the fitted isosbestic signal (*F*0) and the calcium-dependent signals (*F*) with the formula $(F - F0)/F0 \times 100$. Trials with excessive noise or motion artifacts were excluded. To control for differences in jGCaMP7f expression levels between animals, we calculated the *z* score. For this, the entire %Δ*F*/*F*0 signal over the rotarod trial was divided by the standard deviation of the baseline period. For the open field, the *z* score was calculated using the standard deviation of the entire trial. For the peak analysis, the *z* score data were smoothed to reduce noise, allowing for more accurate peak detection.

Behavior Analysis

We used DeepLabCut[24] to track paw position on the rotarod and the position of the mouse in the open field. A small number of trials had missing or disrupted video data and were excluded. Data files generated by DeepLabCut were further analyzed in MATLAB. Scripts can be found at https://github.com/orgs/ubcbraincircuits/repositories

Statistics

Statistical analysis was conducted using GraphPad Prism (San Diego, CA). Two-way analysis of variance (ANOVA) repeated measures with Tukey's multiple comparisons test and unpaired *t* tests were used to compare group data. Mixed-effects analysis was used instead of ANOVA when there were missing values. Pearson's *r* correlation test was used to analyze correlations between behavior and photometry measures, and Fisher's *z* test of correlations was used to compare between correlations.[25]

Results

Characterization of the Striatal Calcium Signal

To measure striatal activity in vivo, we delivered AAV-syn-jGCaMP7f to the striatum, where it was expressed nonspecifically in neurons, and implanted a fiber-optic cannula (Fig. 1A–C; Figure S1). Because >95% of striatal neurons are SPNs, the majority of our jGCaMP7f signals reflect activity in the dendrites and soma of SPNs with much smaller contributions from interneurons and axon terminals that synapse onto striatal cells. At least 2 weeks after surgery, the mice showed extensive expression of jGCaMP7f in the dorsal striatum (Fig. 1B). During open-field exploration, the mice showed peaks in jGCaMP7f activity in response to 465 nm excitation, but little activity in response to 405 nm excitation (Fig. 1D), providing assurance that the latter is a reliable control for basal jGCaMP7f fluorescence and motion artifacts. Green fluorescent protein (GFP) controls were conducted in three animals and showed minimal activity during open field (Fig. 1D) and accelerating rotarod (not shown).

Early in training, we observed a large elevation in jGCaMP7f activity during the rotarod trial in the 2- to 3-month-old WT mice (ie, day 1; Fig. 1E), which fell below baseline following the task. By day 4, jGCaMP7f activity still increased at trial start but quickly diminished, and the mean *z* score during rotarod was significantly reduced compared with early training (Fig. 1E).

Premanifest YAC128 Mice Showed Disrupted Correlation Between Rotarod Performance and Striatal Activity

We aimed to determine how striatal neural activity is affected in YAC128 mice in vivo and how this correlates with behavior in the following two age groups: 2 to 3 months (premanifest) and 6 to 7 months (manifest). The premanifest YAC128 mice had no impairment in latency to fall from the rotarod, and both WT and YAC128 groups significantly improved over training (Fig. 2A). Interestingly, the premanifest YAC128 mice were less likely to rotate than fall from the rotarod and turned around to face the opposite direction more often during trials than WT littermates (Fig. 2B,C; Videos S1–S3). Mean calcium activity (*z* score) during rotarod significantly diminished over training in both genotypes (Fig. 2D,E); however, the YAC128 mice showed lower mean calcium activity than WT (Fig. 2D, E). In the WT animals, we found a strong inverse correlation between latency to fall and *z* score ($r = -0.8057$; Fig. 2F), indicating that as mice improve on the task, overall neuronal activity diminishes. In the YAC128 mice, this correlation ($r = -0.4852$; Fig. 2G) was significantly weaker than WT (Fisher's *z* test $P < 0.001$). Thus, although premanifest YAC128 mice remained on the rotarod for a similar duration to WT, the underlying striatal activity was altered.

Premanifest YAC128 Mice Displayed Aberrant Paw Kinematics and Striatal Activity on the Rotarod

We tracked the vertical position of the hind paws and defined paw slips as instances when one or both hind

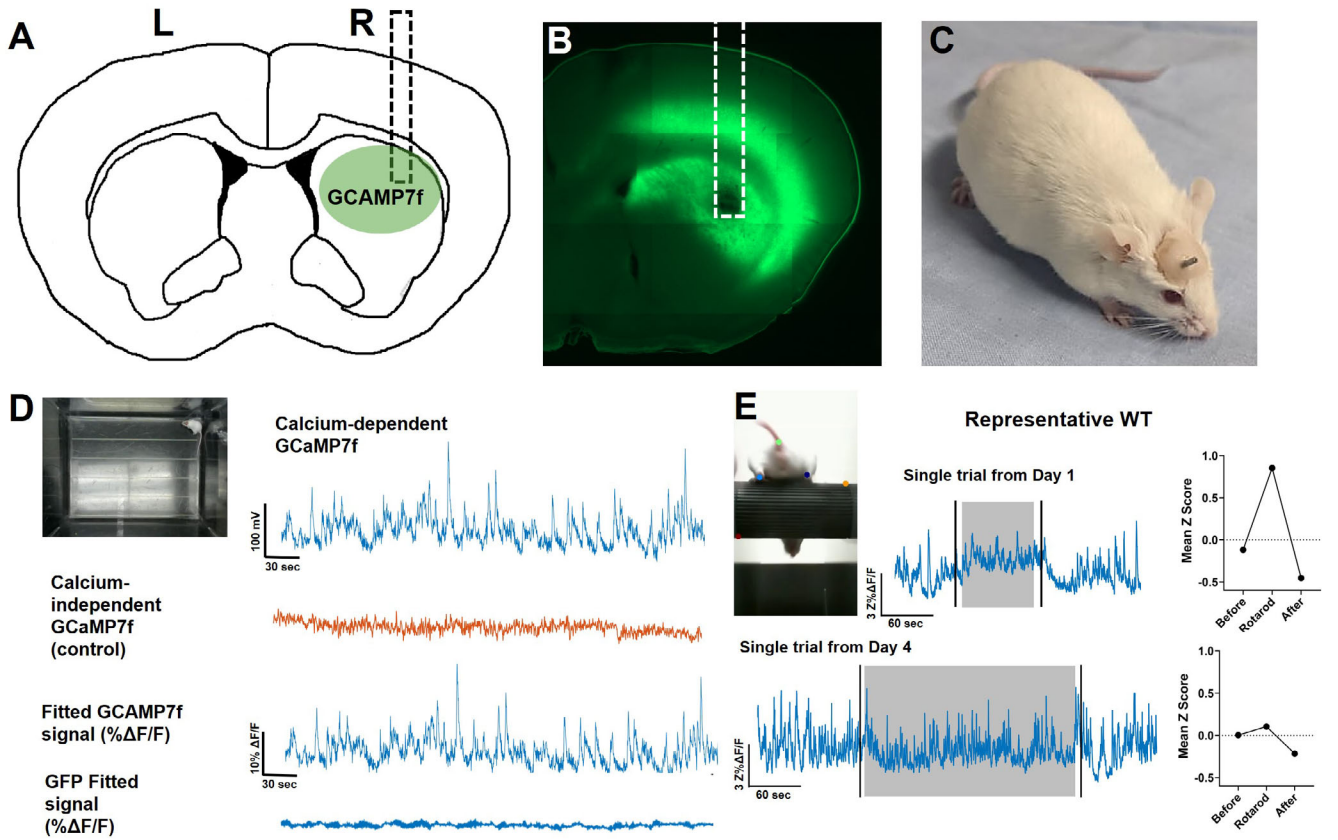

FIG. 1. Characterization of the striatal jGCaMP7f signal. (**A**) Cartoon showing the approximate location of the jGCaMP7f injection and fiber-optic cannula implant (dotted line) in the dorsal striatum. (**B**) Brain slice with jGCaMP7f expression and fiber tract from an experimental animal. (**C**) FVB/N mouse with a fiber-optic cannula implanted in the dorsal striatum. Dental cement is used to adhere the fiber to the skull. (**D**) Example fiber photometry signal from WT mouse during open-field exploration. Top left: Image of mouse in the open field. Top right: Raw jGCaMP7f signal excited at 465 nm to detect calcium-dependent signals. Second row: Raw isosbestic control signals excited at 405 nm to detect calcium-independent signals. Third row: Fitted jGCaMP7f signal showing percentage change in fluorescence. Bottom row: Fitted GFP signal (negative control) showing percentage change in fluorescence. (**E**) Example WT fiber photometry signal during rotarod. Top left: Image of mouse performing the rotarod task. Top middle: Example jGCaMP7f change in fluorescence from a trial on day 1. Black vertical lines denote when mouse is picked up from and returned to empty cage before and after trial. Gray area represents when mouse is on the accelerating rotarod. Top right: Quantification of mean jGCaMP7f data during phases of the trial. Bottom: Example jGCaMP7f change in fluorescence from a trial on day 4 and the quantification of this data during phases of trial. L, left; R, right; WT, wild type. [Color figure can be viewed at wileyonlinelibrary.com]

paws fell below the bottom of the rotarod (Fig. 3A; Videos S4–S7). We found that paw slips decreased over training in both genotypes, but YAC128 mice showed a higher frequency of paw slips (Fig. 3B), especially on day 3 (Fig. 3C).

Next, calcium activity was aligned to each paw slip and averaged per animal. We used a minimum threshold for paw slips of 1.5 cm below the rotarod. For most WT animals, striatal activity ramped up before the slips, followed by a larger increase in activity during and/or following the slips. This effect was more robust for left paw slips than right (Fig. 3D), consistent with recording from the right striatum, where responses are expected to better correlate with movement of the left side of the body.[26] We separated paw slips into early (days 1 and 2) and late training (days 3 and 4). During early training, striatal activity did not show the same increase in WT animals as we noted for all days; however, in late training, we found a large ramping up of activity 1 second before the paw slip, which then slowly declined (Fig. 3E). In contrast, premanifest YAC128 mice showed higher striatal activity associated with paw slips in early training and, strikingly, no increase in activity for paw slips in late training, but instead showed a modest reduction in activity immediately following the slip (Fig. 3E).

Because the rotarod was accelerating throughout the trial, the animals' steps became faster and paw slips became larger and more frequent as the trial progressed (Videos S4–S7). We next classified paw slips as early/slow (0–150 seconds of trial) or late/fast (150 seconds–end). The number of paw slips during the early/slow portion decreased between days 1 and 3 in both genotypes (Fig. S3A,B). Late/fast paw slips were more frequent on day 3 than day 1, owing to increased time on the rotarod in both groups, but the YAC128 mice had a greater number of paw slips on day 3 than the WT (Fig. S3C). We observed a larger increase in activity

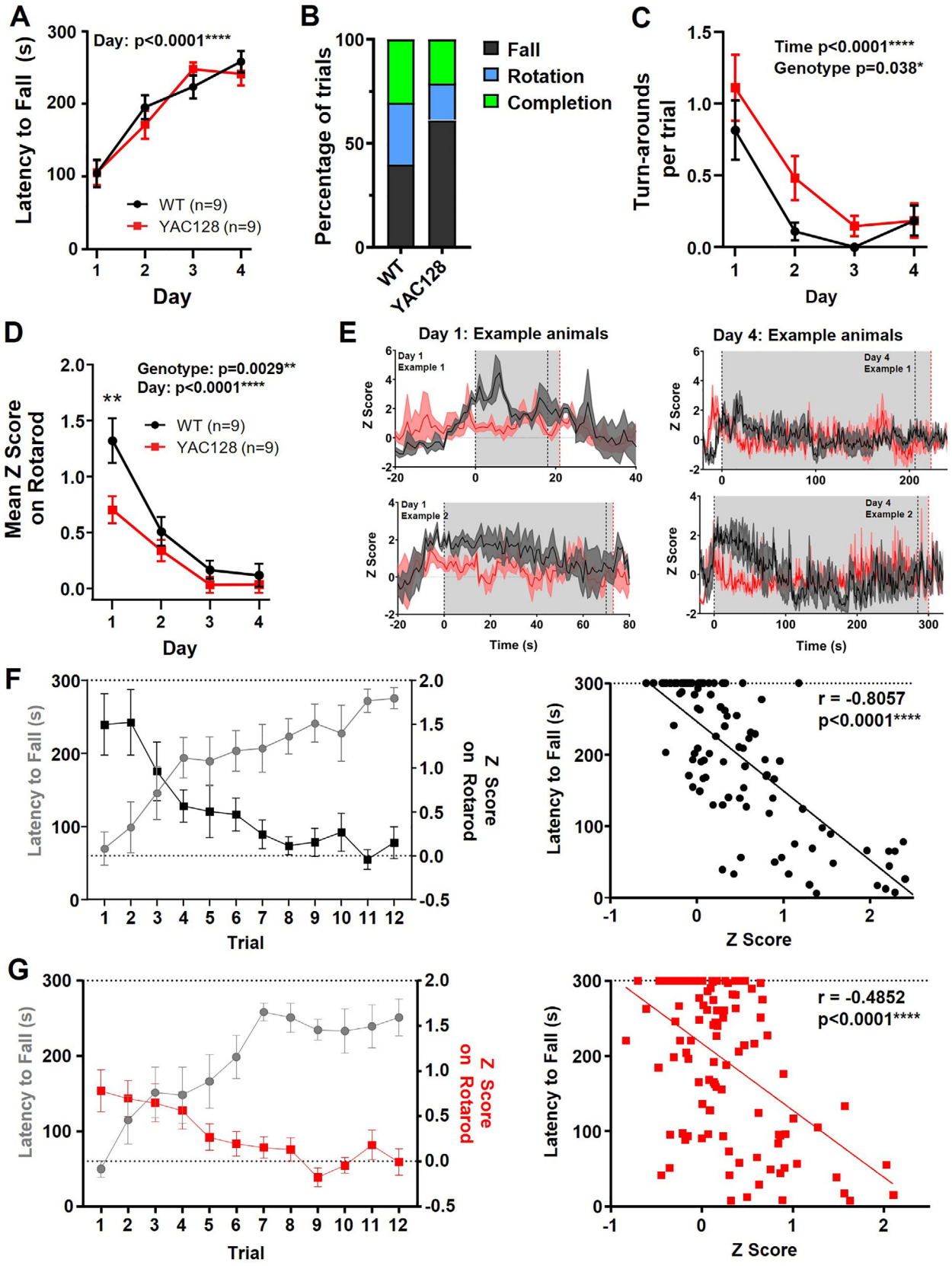

FIG. 2. Legend on next page.

before and after the late/fast paw slips compared with early/slow paw slips for the 2- to 3-month-old WT animals (Fig. S2B,D). However, similar to our observations during late training, YAC128 showed a dip in activity following late/fast slips (Fig. S2D). In addition, both genotypes showed increased paw height with training (Fig. 3F,G) and decreased paw height variability (Fig. 3H), but the YAC128 mice had enhanced variability in paw height on day 3 compared with WT (Fig. 3H).

Manifest YAC128 Mice Exhibited Rotarod Deficits and Elevated Striatal Activity

We also tested 6- to 7-month-old YAC128 mice (manifest). These mice showed severe impairment on the rotarod (Fig. 4A). Both WT and YAC128 at this age ended trials by falling more often than rotating (Fig. 4B). For paw slip analysis, we focused on the first 10 seconds on the rotarod because of the short latency to fall in many manifest YAC128 mice and found significantly increased paw slips in the YAC128 mice (Fig. 4C). Paw height and standard deviation were also markedly altered in the YAC128 mice (Fig. 4D,E).

We separated the YAC128 mice into the following two groups to assess striatal activity associated with sufficient task performance based on the median time on the rotarod of more than or less than 20 seconds: good performers (GP) and poor performers (PP). The GP YAC128 mice were still significantly impaired for latency to fall (Fig. 4F). In addition, mean jGCaMP7f activity on the rotarod was significantly increased for the GP YAC128 group compared with WT (Fig. 4G).

YAC128 Mice Had Disrupted Striatal Activity During Open Field

Mice tested in the open field did not show any difference in center time (not shown) or total distance traveled compared with WT littermates in either age of YAC128 mice (Fig. 5A,C). However, there was a deficit in open-field habituation in manifest YAC128 mice (Fig. 5C). Next, we investigated how striatal activity was affected by analyzing properties of calcium events (peaks). There were no overall differences in peak frequency, amplitude, or width between genotypes (not shown); however, we did find differences in the correlation between peak frequency and behavior for individual mice. WT animals showed a significant correlation between peak frequency and total distance traveled in the open field ($r = 0.46$ at 2–3 months; $r = 0.80$ at 6–7 months), and this correlation was absent in YAC128 animals at both ages (Fig. 5B,D).

To investigate further, we categorized behavior into the following three types and explored how these behaviors and the underlying striatal activity differed between genotypes (Fig. 5E,F): active (locomotion/rearing at wall), grooming, and rest. On day 1, mice were active for the majority of time (60%–80%), whereas grooming accounted for 1% to 10% of total time for most mice (Fig. 5E). Active bouts were longer than grooming and rest for all groups except manifest YAC128 (Fig. 5E). Interestingly, we found a higher peak frequency in striatal activity when mice were at rest in premanifest YAC128 compared with WT mice and a trend for this in manifest YAC128 mice (Fig. 5F).

Because manifest YAC128 animals showed impaired open-field habituation (Fig. 5C), we examined whether this was reflected in the types of behaviors they engaged in. Compared with day 1, on day 3 WT animals reduced the percentage of time spent being active and increased rest (Fig. S3A–C). The manifest YAC128 mice did not show this difference, engaging in similar behaviors on both days (Fig. S3A–C). Average bout duration for the behaviors showed a similar pattern between days and genotypes (Fig. S3D–F). Thus, WT mice modulated their behavior by increasing rest and decreasing activity while manifest YAC128 failed to make these changes.

Discussion

We uncovered multiple ways striatal activity is aberrant during behavior in YAC128 mice as well as previously unknown deficits in paw kinematics in these animals starting as early as 2 to 3 months of age.

Rotarod Deficits and Paw Kinematics in Premanifest and Manifest YAC128 Mice

At 2 to 3 months, the YAC128 mice show mild behavioral deficits,[7,8] similar to the prodromal phase for patients with HD, when subtle motor impairments start to appear.[27–29] Our premanifest YAC128 cohort did not show any deficit in latency to fall on the accelerating rotarod, which mirrors results from previous

FIG. 2. Changes to rotarod performance and striatal activity on the rotarod in premanifest YAC128 mice. (**A**) Latency to fall over days of training (three trials averaged per day) (day effect, $P < 0.0001$; two-way analysis of variance [ANOVA]). (**B**) Percentage of trials that ended by falling, rotating, or completing full trial. (**C**) Mean number of turnarounds per trial over days of training (day effect, $P < 0.0001$; genotype effect, $P = 0.0038$; two-way ANOVA). (**D**) Mean *z* score on rotarod over days of training (day effect, $P < 0.0001$; genotype effect, $P = 0.0029$; and genotype difference on day 1, $P = 0.0010$; two-way ANOVA with multiple comparisons). (**E**) jGCaMP7f traces from two example animals of each genotype. Each trace is the average of three trials for day 1 (left) and day 4 (right). Gray area denotes average latency to fall that day for WT (black dotted line) and YAC128 (red dotted line). (**F–G**) Left: Latency to fall plotted against mean *z* score per trial for WT (**F**) and YAC128 (**G**). Right: Scatterplot of latency to fall compared with *z* score for each trial (WT, Pearson's $r = -0.8057$, $P < 0.0001$; YAC128 Pearson's $r = -0.4852$, $P < 0.0001$). WT, wild type; YAC128, yeast artificial chromsome-128CAG. [Color figure can be viewed at wileyonlinelibrary.com]

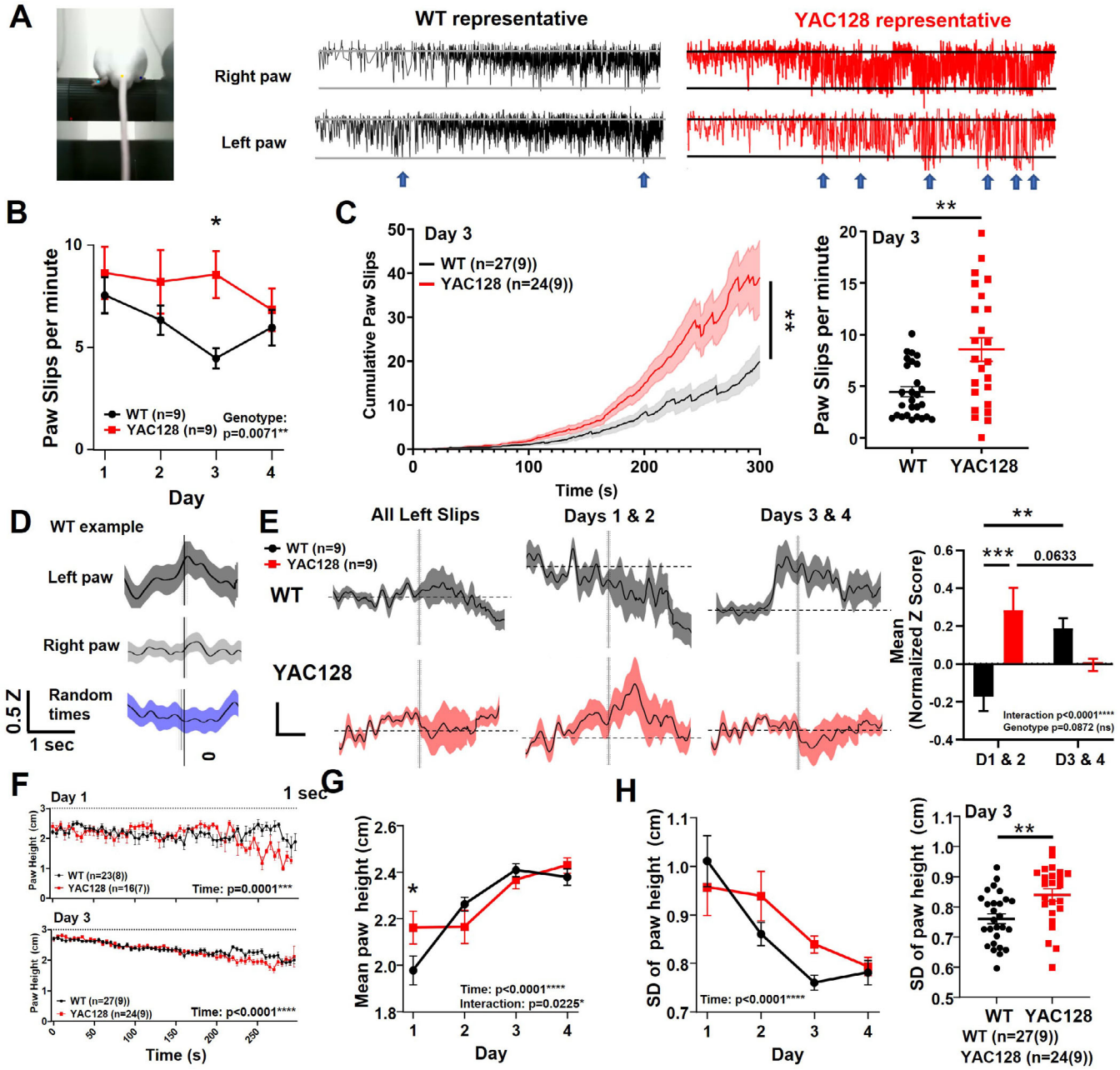

FIG. 3. Paw kinematics and striatal activity during paw slips in premanifest YAC128 mice. (**A**) Mouse on rotarod with labeled hindpaws, and WT and YAC128 representative examples of vertical paw position over time. Blue arrows indicate some paw slips. (**B**) Paw slips per minute over days of training (genotype effect, $P = 0.0071$; genotype difference on day 3, $P = 0.0114$; denoted by *; two-way analysis of variance [ANOVA] multiple comparisons). (**C**) Left: Cumulative paw slips over time during rotarod trials on day 3 (mixed-effects analysis, genotype, $P = 0.0073$; time, $P < 0.0001$; denoted by **). Three YAC128 trials were excluded because of missing or disrupted video data. Right: Day 3 mean paw slips/trial (unpaired *t* test, $P = 0.0013$). (**D**) Example of normalized jGCaMP7f *z* score data from WT animal for all paw slips on rotarod. The *z* score (Z) is normalized by subtracting baseline period (Z0) of 3 to 1 second before the paw slips (Z − Z0). Vertical line represents paw slip or random time that data were aligned with. (**E**) Left: Normalized *z* score was calculated for each animal and averaged per genotype. Middle left: Normalized *z* score for paw slips on days 1 and 2. Two YAC128 animals were excluded because of insufficient number of paw slips (<3 paw slips total for days 1 and 2 combined). Middle right: Normalized *z* score for paw slips on days 3 and 4. Right: Mean normalized *z* score from −1 to +3 second time points around paw slips (interaction, $P = 0.0001$; genotype, $P = 0.0872$; genotype comparison on days 1/2, $P = 0.0009$; denoted by ***; WT days comparison, $P = 0.0079$; denoted by **; YAC128 days comparison, $P = 0.0633$). (**F**) Paw height (both paws) over trial duration for day 1 (top) and day 4 (bottom; number of trials shown with number of animals in brackets; time effect, $P < 0.0001$; two-way ANOVA). (**G**) Mean paw height over days of training (time effect, $P < 0.0001$; interaction, $P = 0.0225$; genotype day 1, $P = 0.0461$). (**H**) Left: Standard deviation of paw height over days of training (time effect, $P < 0.0001$). Right: Standard deviation of paw height per trial (both paws averaged) on day 3 ($P = 0.0037$, denoted by **, unpaired *t* test). ns, nonsignificant; WT, wild type; YAC128, yeast artificial chromsome-128CAG. [Color figure can be viewed at wileyonlinelibrary.com]

work.[8] Interestingly, the premanifest YAC128 mice were more likely to fall off than make a full rotation around the rotarod. This difference could reflect a motor control deficit or impaired grip strength, as shown in other HD models.[30] Turnaround behavior decreased with training; however, the YAC128 mice

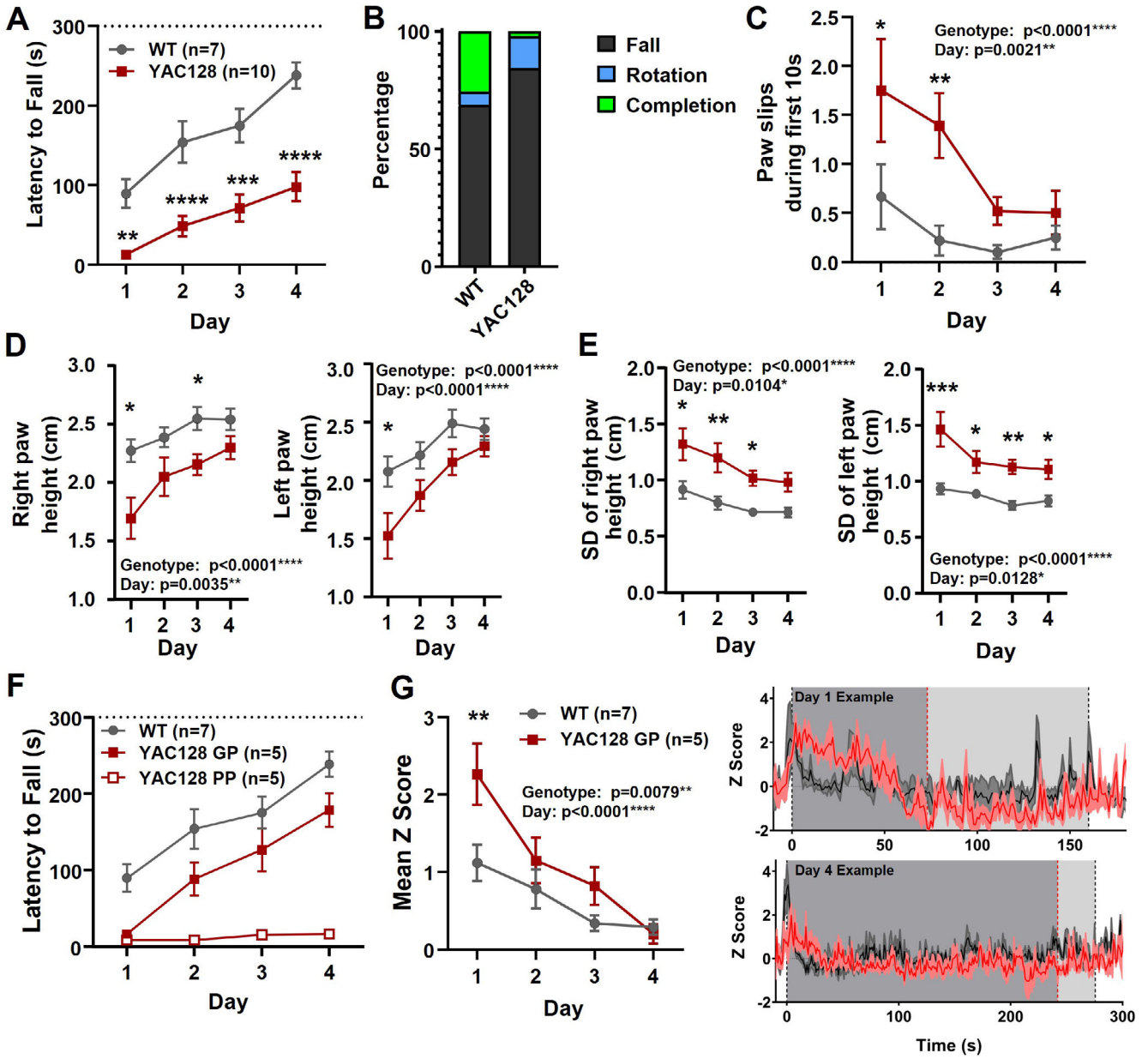

FIG. 4. Manifest YAC128 mice: performance and striatal activity during rotarod. (**A**) Latency to fall over days of training for manifest YAC128 compared with WT (genotype, $P < 0.0001$; time, $P < 0.0001$; multiple comparisons: day 1, $P = 0.0072$, denoted by **; day 2, $P < 0.0001$, denoted by ****; day 3, $P = 0.0001$, denoted by ***; day 4, $P < 0.0001$, denoted by ****). (**B**) Percentage of trials where mice fell, rotated, or completed the full duration. (**C**) Paw slips during the first 10 seconds for WT and manifest YAC128 over days of training (genotype, $P < 0.0001$; day, $P = 0.0021$; multiple comparisons: day 1, $P = 0.0335$, denoted by *, day 2, $P = 0.0034$, denoted by **). (**D**) Right and left paw heights over days of training (genotype, $P < 0.0001$ both paws; day: right paw, $P = 0.0035$; left paw, $P < 0.0001$; multiple comparisons day 1: right, $P = 0.0118$, denoted by *, left, $P = 0.0271$, denoted by *; day 3: right, $P = 0.0486$, denoted by *). (**E**) SD of right and left paw height (genotype, $P < 0.0001$ both paws; day: right paw, $P = 0.0104$, left paw, $P = 0.0128$; multiple comparisons day 1: right, $P = 0.0194$, denoted by *, left, $P = 0.0001$, denoted by ***; day 2: right, $P = 0.0034$, denoted by **, left, $P = 0.0255$, denoted by *; day 3: right, $P = 0.0342$, denoted by *, left, $P = 0.0028$, denoted by **; day 4: left, $P = 0.0233$, denoted by *). (**F**) Latency to fall for WT, and YAC128 GP and PP (group, $P < 0.0001$; day, $P < 0.0001$; interaction, $P = 0.0030$). (**G**) Left: Mean *z* score on rotarod over days of training in WT and GP YAC128 (genotype, $P = 0.0079$; day, $P < 0.0001$). Right: Examples from one WT and one GP YAC128 showing jGCaMP7f traces (three trials averaged) on day 1 (top) and day 4 (bottom). Gray areas denote approximate times when mice are on the rotarod based on daily mean latency to fall (YAC128, dark gray; WT, light gray). Dotted lines indicate mean latency to fall of the three trials (YAC128, red; WT, black). GP, good performers; PP, poor performers; SD, standard deviation; WT, wild type; YAC128, yeast artificial chromsome-128CAG. [Color figure can be viewed at wileyonlinelibrary.com]

displayed a higher number of turnarounds, which could reflect impaired learning of the correct strategy for the task or hyperactivity, as reported in early-stage YAC128 mice in other behavioral tests.[7,8] We also showed higher paw slip frequency and increased paw height variability in premanifest YAC128 mice. In C57/B6 mice, previous studies have shown increased paw height and decreased variability with training on

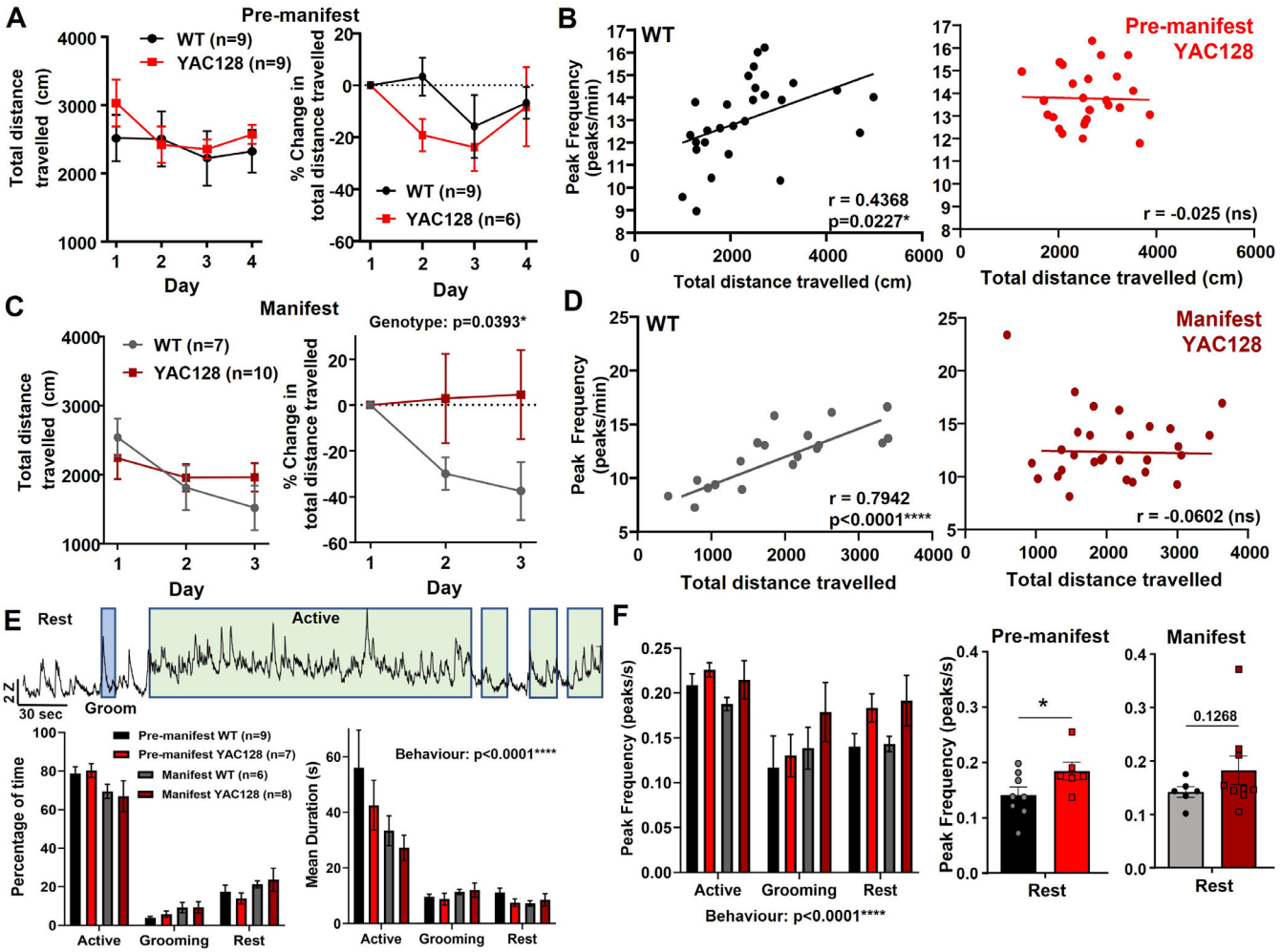

FIG. 5. Behavior and striatal activity during open field in WT and YAC128 mice. (**A**) Total distance traveled (left) and change in distance traveled from day 1 (right) in premanifest YAC128 and their WT littermates. Three premanifest YAC128 mice were excluded from change in total distance analysis because of missing or disrupted behavior videos on day 1. (**B**) Scatterplots of calcium peak frequency and total distance traveled for each open-field trial in WT (left, $r = 0.4368$, $P = 0.0227$) and YAC128 (right, no significant correlation). Of the WT trials, 25% (nine) and 27% (10) of YAC128 trials were excluded from correlation analysis because of disruptions to behavior video data or photometry data. (**C**) Total distance traveled (left) and change in distance traveled from day 1 (right) in manifest YAC128 and their WT littermates. Significant genotype effect for change in distance traveled ($P = 0.0393$, two-way analysis of variance). (**D**) Scatterplots of calcium peak frequency and total distance traveled for each open-field trial in WT (left, $r = 0.7942$, $P < 0.0001$) and YAC128 (right, no significant correlation). Of the WT trials, 10% (two) and 3% (one) of YAC128 trials were excluded from correlation analysis because of disruptions to video data or photometry data. (**E**) Top: Example jGCaMP7f activity trace from an open-field trial (2- to 3-month-old WT) showing periods of active behavior (green), grooming behavior (blue), and the other periods are rest behavior. Bottom left: Percentage of time spent in the active, grooming, or rest behavior for premanifest and manifest YAC128 and WT littermates (behavior, $P < 0.0001$). All groups showed a significantly higher percentage of time spent active compared with grooming or rest behavior ($P < 0.0001$ for comparisons between behaviors for all four groups). Bottom right: Average duration per bout of each behavior for premanifest and manifest YAC128 and WT littermates (behavior, $P < 0.0001$). All groups except manifest YAC128 showed a significantly higher bout duration for active versus grooming and rest behaviors (premanifest WT: $P < 0.0001$ active vs. rest and active vs. grooming; premanifest YAC128: $P = 0.0004$ active vs. grooming, $P = 0.0002$ active vs. rest; manifest WT: $P = 0.0325$ active vs. grooming, $P = 0.0082$ active vs. rest). (**F**) Left: Calcium peak frequency (per second) during different behaviors (behavior, $P = 0.0003$; genotype, $P = 0.0818$). Middle: Peak frequency at rest for premanifest YAC128 and WT ($P = 0.0341$, denoted by *, unpaired t test). Right: Peak frequency at rest for manifest YAC128 and WT ($P = 0.1268$, unpaired t test). ns, nonsignificant; WT, wild type; YAC128, yeast artificial chromsome-128CAG. [Color figure can be viewed at wileyonlinelibrary.com]

the rotarod,[16,17] indicating that these kinematic features are refined with learning. We found that initial paw slip frequency and height variability are similar to WT in the premanifest YAC128 mice but diverge by day 3, suggesting impaired motor refinement.

By 6 to 7 months, the YAC128 mice showed severe kinematic deficits, including increased paw slip frequency, reduced paw height, and increased variability accompanied by a marked deficit in latency to fall. Impaired motor refinement has been shown in HD models for other tasks, including research from our group showing that 10- to 11-month-old Q175/FDN HD mice were impaired at learning a forelimb lever-pulling task.[31] Our manifest YAC128 mice performed worse than expected,[7,8] which could be attributed to the added difficulty of performing the task while

tethered by a fiber-optic patch cord. This may have exacerbated motor deficits as well as worsening motivation deficits and apathy-like behavior, which have been shown in HD mice.[32,33] In sum, our behavioral results reveal progressive deficits in paw kinematics and motor refinement on the rotarod in YAC128 mice.

Striatal Activity During Rotarod Performance

For both WT and YAC128 animals, we saw a strong reduction in overall striatal activity by day 4 of rotarod training. Kupferschmidt and colleagues found a similar activity increase above baseline that diminished with rotarod training in cortical inputs to the striatum.[17] There is evidence that with learning, the striatum recruits task-specific neuronal ensembles similar to those observed in the motor cortex.[16,34] During rotarod training, neurons important for refining movement are likely potentiated, whereas those not important for the task are likely inhibited, suggesting that only those ensembles important for rotarod performance remain active by late training. This could explain the lower striatal activity we observed on day 4 compared with day 1. Costa and colleagues showed that the number of newly recruited neurons decreased over 3 days of rotarod training, whereas the number of neurons no longer activated during the task increased.[14] Future studies using techniques to visualize individual neurons, such as activity-dependent protein expression (see, eg, Cao and colleagues[16]) or miniscope imaging,[35] could help determine whether specific neuronal ensembles in the striatum are consolidated during rotarod learning.

YAC128 Mice Displayed Changes to Striatal Activity During Rotarod Performance

Premanifest YAC128 animals showed lower striatal activity on day 1 of training and a weaker inverse correlation between striatal activity and latency to fall compared with WT. This attenuated change in striatal activity over successive rotarod trials in premanifest YAC128 mice suggests impaired synaptic plasticity. Moreover, although both genotypes remained on the rotarod for a similar duration, aberrant motor coordination in the YAC128 mice may be associated with fluctuations in striatal activity that are not present in WT animals. Alternatively, other areas of the brain, such as the motor cortex, may compensate for disrupted striatal activity to improve performance. Furthermore, we found a different pattern of neuronal activity surrounding paw slip events; the absence of increased striatal activity associated with paw slips in late training may also indicate a deficit in synaptic plasticity in the YAC128 mice, resulting in an impaired ability to refine behavior.

The majority of neurons in the striatum are gamma-aminobutyric acid (GABA) ergic SPNs of the following two types: D1-SPNs, which express dopaminergic D1 receptors and project to the direct pathway, and D2-SPNs, which express D2 receptors that project to the indirect pathway.[36] In HD, the D2-SPNs preferentially degenerate early in the disease, and D1-SPNs degenerate later.[5,6,37] Early-stage HD mouse models display evidence of higher D1-SPN activity, which could occlude synaptic plasticity associated with motor learning.[38–41] Corticostriatal synaptic plasticity on D2-SPNs is also implicated in motor learning[11] and shows early deficits in HD mice.[10,40] The competitive model for striatal action selection suggests that the balance of synaptic plasticity in ensembles of D1- and D2-SPNs determines behavioral output,[34] thus disruptions to this balance in YAC128 likely contribute to impaired rotarod learning.

Manifest YAC128 mice categorized as GP showed significantly higher striatal activity on the rotarod and performed worse than their WT littermates. Elevated neuronal activity could result from altered glutamatergic signaling, disrupting the balance of SPN activity and leading to motor deficits. Changes to glutamate transmission have been reported in YAC128 mice, including increased extrasynaptic N-methyl-D-aspartate receptor (NMDAR) expression and currents, and blocking extrasynaptic NMDAR-rescued rotarod deficits in YAC128 mice.[42] In manifest YAC128 mice, reduced synaptic glutamate currents and lower spontaneous activity of D1-SPNs have been reported.[38,41] Antagonism of D1 receptors has been shown to disrupt rotarod learning,[2] so lower D1-SPN activity at manifest stages, perhaps in conjunction with other changes to glutamate transmission, could lead to rotarod impairments.

YAC128 Mice Showed Altered Behavior and Striatal Activity During Open Field

WT mice showed a positive correlation between frequency of striatal calcium events and total distance traveled in the open field; however, there was no correlation between these measures in premanifest or manifest YAC128 mice. Manifest YAC128 mice also showed a deficit in open-field habituation, indicating memory impairments, consistent with previous work.[8] Intriguingly, the premanifest YAC128 mice exhibited a significantly higher calcium peak frequency at rest compared with WT. Previous work has shown an increased SPN firing rate in freely behaving R6/2 HD mice and reduced correlated firing between pairs of neurons.[21] The increased peak frequency we observed at rest could contribute to the disrupted correlation between distance traveled and peak frequency in YAC128 mice. Increased spontaneous activity of D1-SPNs could be driving the increased peak frequency we observed, as elevated spontaneous excitatory postsynaptic currents

(sEPSCs) have been shown in vitro in early-stage HD mice.[38,41] It will thus be important to investigate signaling of D1- and D2-SPNs separately during behavior to determine the role of these two pathways.

Conclusions

Here we demonstrate disruptions to striatal activity that correlate with aberrant behavior on the accelerating rotarod and open field in YAC128 mice. We provide the first reported analysis of paw kinematics during rotarod in an HD mouse model, a useful readout to detect early motor deficits. Fiber photometry also provides an ideal platform for testing pharmacological interventions on both behavior and the underlying neural activity in disease models. Using these tools, interventions could be tested starting at early stages to prevent the progression of motor deficits.

Acknowledgments: We thank Lily Zhang and Pumin Wang for performing surgeries, and Ryan Yeung, Evan Fung, Jean Oh, and Amy Smith-Dijak for assistance with data analysis. We are grateful to Drs. Jaideep Bains, David Rosenegger, and Tamas Fuzesi for providing expert advice in setting up our fiber photometry system. This work was supported by resources made available through the Dynamic Brain Circuits cluster, DataBinge, and the NeuroImaging and NeuroComputation Centre at the University of British Columbia Djavad Mowafaghian Centre for Brain Health (RRID SCR_019086). Operating funds were provided by Canadian Institutes of Health Research Foundation Grant 143210 to L.A.R. in addition to support from the Brain Canada Platform grant Optogenetics Vectorology Foundry. Equipment for this study was purchased through a Canadian Foundation for Innovation John Evans Leadership Foundation award to L.A.R.

Data Availability Statement

The data that support the findings of this study are available from the corresponding author upon reasonable request.

References

1. Kreitzer AC, Malenka RC. Striatal plasticity and basal ganglia circuit function. Neuron 2008;60:543–554.
2. Yin HH, Mulcare SP, Hilário MRF, et al. Dynamic reorganization of striatal circuits during the acquisition and consolidation of a skill. Nat Neurosci 2009;12:333–341.
3. Dayan E, Cohen LG. Neuroplasticity subserving motor skill learning. Neuron 2011;72:443–454.
4. Balleine BW, O'Doherty JP. Human and rodent homologies in action control: corticostriatal determinants of goal-directed and habitual action. Neuropsychopharmacol 2010;35:48–69.
5. Bates GP, Dorsey R, Gusella JF, et al. Huntington disease. Nat Rev Dis Primer 2015;1:15005
6. Ross CA, Tabrizi SJ. Huntington's disease: from molecular pathogenesis to clinical treatment. Lancet Neurol 2011;10:83–98.
7. Slow EJ, van Raamsdonk J, Rogers D, et al. Selective striatal neuronal loss in a YAC128 mouse model of Huntington disease. Hum Mol Genet 2003;12:1555–1567.
8. Raamsdonk JMV, Pearson J, Slow EJ, Hossain SM, Leavitt BR, Hayden MR. Cognitive dysfunction precedes neuropathology and motor abnormalities in the YAC128 mouse model of Huntington's disease. J Neurosci 2005;25:4169–4180.
9. Raymond LA, André VM, Cepeda C, Gladding CM, Milnerwood AJ, Levine MS. Pathophysiology of Huntington's disease: time-dependent alterations in synaptic and receptor function. Neuroscience 2011;198:252–273.
10. Sepers MD, Smith-Dijak A, LeDue J, Kolodziejczyk K, Mackie K, Raymond LA. Endocannabinoid-specific impairment in synaptic plasticity in striatum of Huntington's disease mouse model. J Neurosci 2018;38:544–554.
11. Lovinger DM. Neurotransmitter roles in synaptic modulation, plasticity and learning in the dorsal striatum. Neuropharmacology 2010;58:951–961.
12. Koch ET, Raymond LA. Dysfunctional striatal dopamine signaling in Huntington's disease. J Neurosci Res 2019;97:1636–1654.
13. Cepeda C, Murphy KPS, Parent M, Levine MS. Chapter 10 - the role of dopamine in Huntington's disease. In: Diana M, Di Chiara G, Spano P, eds. Progress in Brain Research. Amsterdam: Elsevier; 2014:235–254.
14. Costa RM, Cohen D, Nicolelis MAL. Differential Corticostriatal plasticity during fast and Slow motor skill learning in mice. Curr Biol 2004;14:1124–1134.
15. Benthall KN, Cording KR, Agopyan-Miu AHCW, Wong CD, Chen EY, Bateup HS. Loss of Tsc1 from striatal direct pathway neurons impairs endocannabinoid-LTD and enhances motor routine learning. Cell Rep 2021;36:109511
16. Cao VY, Ye Y, Mastwal S, et al. Motor learning consolidates arc-expressing neuronal ensembles in secondary motor cortex. Neuron 2015;86:1385–1392.
17. Kupferschmidt DA, Juczewski K, Cui G, Johnson KA, Lovinger DM. Parallel, but dissociable, processing in discrete Corticostriatal inputs encodes skill learning. Neuron 2017;96:476–489.e5.
18. Hong SL, Cossyleon D, Hussain WA, Walker LJ, Barton SJ, Rebec GV. Dysfunctional behavioral modulation of corticostriatal communication in the R6/2 mouse model of Huntington's disease. PLoS ONE 2012;7:e47026
19. Rothe T, Deliano M, Wójtowicz AM, et al. Pathological gamma oscillations, impaired dopamine release, synapse loss and reduced dynamic range of unitary glutamatergic synaptic transmission in the striatum of hypokinetic Q175 Huntington mice. Neuroscience 2015;311:519–538.
20. Naze S, Humble J, Zheng P, Barton S, Rangel-Barajas C, Rebec GV, Kozloski JR. Cortico-striatal cross-frequency coupling and gamma genesis disruptions in Huntington's disease mouse and computational models. ENeuro 2018;5(6):ENEURO.0210-18.
21. Miller BR, Walker AG, Fowler SC, von Hörsten S, Riess O, Johnson MA, Rebec GV. Dysregulation of coordinated neuronal firing patterns in striatum of freely behaving transgenic rats that model Huntington's disease. Neurobiol Dis 2010;37:106–113.
22. Friedman A, Hueske E, Drammis SM, et al. Striosomes mediate value-based learning vulnerable in age and a Huntington's disease model. Cell 2020;183:918–934.e49.
23. Parsons MP, Vanni MP, Woodard CL, Kang R, Murphy TH, Raymond LA. Real-time imaging of glutamate clearance reveals normal striatal uptake in Huntington disease mouse models. Nat Commun 2016;7:11251
24. Mathis A, Mamidanna P, Cury KM, Abe T, Murthy VN, Mathis MW, Bethge M. DeepLabCut: markerless pose estimation of user-defined body parts with deep learning. Nat Neurosci 2018;21:1281–1289.
25. Weiss, BA. Fisher's Z Transformation [Computer Software]. 2011. Available from: https://blogs.gwu.edu/weissba/teaching/calculators/fishers-z-transformation/
26. Cui G, Jun SB, Jin X, Pham MD, Vogel SS, Lovinger DM, Costa RM. Concurrent activation of striatal direct and indirect pathways during action initiation. Nature 2013;494:238–242.
27. McGarry A, Biglan KM. Chapter 7 - preclinical motor manifestations of Huntington disease. In: Feigin AS, Anderson KE, eds. Handbook of Clinical Neurology. Amsterdam: Elsevier; 2017:93–98.
28. Zhang Y, Zhou J, Gehl CR, et al. Mild cognitive impairment as an early landmark in Huntington's disease. Front Neurol 2021;12:678652

29. Tabrizi SJ, Scahill RI, Owen G, et al. Predictors of phenotypic progression and disease onset in premanifest and early-stage Huntington's disease in the TRACK-HD study: analysis of 36-month observational data. Lancet Neurol 2013;12:637–649.

30. Menalled LB, Kudwa AE, Miller S, et al. Comprehensive behavioral and molecular characterization of a new Knock-in mouse model of Huntington's disease: zQ175. PLOS ONE 2012;7:e49838

31. Woodard CL, Sepers MD, Raymond LA. Impaired refinement of kinematic variability in Huntington disease mice on an automated home cage forelimb motor task. J Neurosci 2021;41:8589–8602.

32. Heath CJ, O'Callaghan C, Mason SL, et al. A touchscreen motivation assessment evaluated in Huntington's disease patients and R6/1 model mice. Front Neurol 2019;10:858

33. Minnig S, Bragg RM, Tiwana HS, et al. Early detection of apathetic phenotypes in Huntington's disease Knock-in mice using open source tools. Sci Rep 2018;8:2304

34. Bariselli S, Fobbs WC, Creed MC, Kravitz AV. A competitive model for striatal action selection. Brain Res 2019;1713:70–79.

35. Stamatakis AM, Resendez SL, Chen K-S, et al. Miniature microscopes for manipulating and recording *in vivo* brain activity. Microscopy 2021;70:399–414.

36. Gerfen CR, Engber TM, Mahan LC, Susel Z, Chase TN, Monsma FJ, Sibley DR. D1 and D2 dopamine receptor-regulated gene expression of striatonigral and striatopallidal neurons. Science 1990;250:1429–1432.

37. Albin RL, Young AB, Penney JB. The functional anatomy of basal ganglia disorders. Trends Neurosci 1989;12:366–375.

38. Andre V, Fisher Y, Levine M. Altered balance of activity in the striatal direct and indirect pathways in mouse models of Huntington's disease. Front Syst Neurosci 2011;5:46

39. Willuhn I, Steiner H. Motor-skill learning in a novel running-wheel task is dependent on D1 dopamine receptors in the striatum. Neuroscience 2008;153:249–258.

40. Plotkin JL, Day M, Peterson JD, et al. Impaired TrkB receptor signaling underlies Corticostriatal dysfunction in Huntington's disease. Neuron 2014;83:178–188.

41. André VM, Cepeda C, Fisher YE, et al. Differential electrophysiological changes in striatal output neurons in Huntington's disease. J Neurosci 2011;31:1170–1182.

42. Milnerwood AJ, Gladding CM, Pouladi MA, et al. Early increase in Extrasynaptic NMDA receptor signaling and expression contributes to phenotype onset in Huntington's disease mice. Neuron 2010;65:178–190.

Supporting Data

Additional Supporting Information may be found in the online version of this article at the publisher's web-site.